MATERIALS CHEMISTRY FRONTIERS

RESEARCH ARTICLE

View Article Online
View Journal

Cite this: DOI: 10.1039/d6qm00097e

One-pot ethanol-mediated synthesis of surface Si-zoned ZSM-5 zeolites

Jiayu Yu,[a] Di Pan,[a] Ke Du,[a] Wei Chen,[a] Jian Zhou,*[b] Yi Tang [a] and Yahong Zhang *[a]

Received 5th February 2026,
Accepted 16th April 2026

DOI: 10.1039/d6qm00097e

rsc.li/frontiers-materials

Passivation of external surface acid sites in zeolites is a widely used strategy to enhance catalytic stability and to mitigate undesired non-shape-selective reactions. However, the synthesis of zeolites with a uniform and thickness-controllable Si-zoned shell in a true one-pot process remains a significant challenge. Here, we develop an ethanol-mediated one-pot route to synthesize surface Si-zoned ZSM-5 zeolites. Ethanol creates a favorable synthesis environment that promotes a classical, layer-by-layer crystallization pathway, enabling the near-quantitative utilization of aluminosilicate species during the initial crystallization stage. This complete consumption of framework-forming species allows soluble silicate species to be subsequently added directly into the mother liquor, where they are selectively incorporated onto the preformed ZSM-5 crystals to build a thickness-tunable silica-rich shell. Notably, bulk and surface analyses together with probe reactions using bulky molecules confirm that the silica-rich shell is structurally continuous and effectively inert toward bulky reactants. This ethanol-mediated strategy offers a facile, high-yield, and scalable one-pot platform for engineering surface compositions in zeolites. The resulting surface Si-zoned ZSM-5 offers a versatile basis for the design of catalysts with improved stability and shape-selectivity.

1. Introduction

ZSM-5 zeolites are widely used as catalytic materials in industry due to their unique acidic properties and nanoporous structures.[1,2] Brønsted acid sites located inside the channels and on external surfaces collectively determine the overall acidity of H-form zeolites, while the well-defined pore system imposes molecular shape-selectivity and thereby enhances product selectivity. However, acid sites on the external surface often lead to a diminished selectivity toward target products and accelerate catalyst deactivation,[3–5] which is further intensified by the surface Al enrichment in zeolites. Notably, such surface Al zoning, that is, an Al-enriched external surface relative to the bulk framework Al concentration, is widely observed in ZSM-5 crystals.[6–8] Therefore, extensive efforts have been devoted to passivating the external surface acidity of ZSM-5, including acid leaching,[9] chemical vapor[10,11] or liquid deposition of silicon compounds,[12,13] deposition of metal oxides or inorganic coatings,[14–16] and growth of silica-rich crystalline layers (*e.g.*, silicalite-1) on the surface.[17–20] Among these approaches, the construction of surface Si-zoned ZSM-5, featuring a Si-enriched outer shell on an Al-containing core, has attracted significant attention. Such materials effectively passivate external surface acid sites while simultaneously mitigating the adverse effects commonly associated with other methods, such as defect formation, pore narrowing, or partial pore blockage.[21,22]

Despite this progress, most reports rely on a two-step core–shell synthetic protocol.[23] In a typical procedure, an Al-containing zeolite core is first synthesized and subjected to washing, drying, or calcining to remove residual species. The pretreated core is then re-dispersed in a separate precursor solution, where an aluminum-free zeolite shell is grown hydrothermally. To promote uniform shell growth and suppress homogeneous nucleation, a high H_2O/SiO_2 ratio (often $>$ 100) is usually required,[24,25] resulting in large volumes of dilute mother liquor and low silica utilization. Conceptually, it is more desired to grow an epitaxial non-acidic zeolite shell on an acidic zeolite core in a single synthesis system, thereby omitting the separation of zeolite core from synthesis system and maximizing the utilization of silica species. However, a true one-pot route to surface Si-zoned ZSM-5 remains highly challenging for at least two reasons. First, one must ensure that all aluminum-containing species are incorporated into the core crystals during the initial crystallization stage. Second, after

[a] *Department of Chemistry, Laboratory of Advanced Materials, College of Smart Materials and Future Energy, Shanghai Key Laboratory of Molecular Catalysis and Innovative Materials, State Key Laboratory of Porous Materials for Separation and Conversion, Fudan University, Shanghai 200433, P. R. China. E-mail: zhangyh@fudan.edu.cn*

[b] *State Key Laboratory of Green Chemical Engineering and Industrial Catalysis, Sinopec Shanghai Research Institute of Petrochemical Technology Co., Ltd, Shanghai, 201208, P. R. China. E-mail: zhouj.sshy@sinopec.com*

core formation, the newly introduced silica source must preferentially crystallize epitaxially around the existing zeolite crystals rather than nucleating homogeneously to form secondary particles. Achieving both criteria simultaneously in a single synthesis batch has rarely been accomplished.

Alcohols, as common organic solvents, have been widely used in zeolite synthesis systems, particularly as pore-filling agents in the synthesis of high-silica zeolites[26] and as modifiers of crystal morphology during growth.[27,28] Notably, in our previous work,[29] we demonstrated that ethanol, when used as a co-solvent, can suppress nonclassical crystallization pathways and significantly promote classical crystallization. This indicates that ethanol can modify the crystallization environment and favor a growth mode at the crystal-solution interface in which soluble silicate species add to existing crystal surfaces in a layer-by-layer manner. Such a growth mode is attractive for surface modification as it facilitates the formation of smooth and conformal shells, while simultaneously suppressing homogeneous nucleation associated with the nonclassical pathway. Motivated by these insights, in this work, we develop an ethanol-mediated one-pot strategy for synthesizing surface Si-zoned ZSM-5 zeolites. Ethanol promotes the initial crystallization stage, driving near-complete incorporation of silicon and aluminum species into ZSM-5 crystals, resulting in an Al-depleted mother liquor. Subsequent addition of soluble silica to the same system, under the continued influence of ethanol, induces classical epitaxial growth of a silica-rich shell with tunable thickness at the crystal surface, yielding ZSM-5 zeolites with well-defined surface Si zoning. The specific preparation route is illustrated in Scheme 1. This integrated ethanol-enabled route provides a one-pot, high-yield synthesis of surface Si-zoned ZSM-5, ensuring near-quantitative utilization of framework-forming species without core isolation while allowing precise control over the thickness and uniformity of the silica-rich shell. These features offer a versatile platform for tailoring external surface composition in zeolites and pave the way for designing ZSM-5-based catalysts with enhanced stability and shape-selective performance.

2. Experimental section

2.1. Chemical and materials

All of the following reagents are directly used without further purification. Tetraethyl orthosilicate (TEOS, $C_8H_{20}O_4Si$, ≥98%, Shanghai Aladdin Biochemical Technology Co., Ltd), Tetrapropylammonium hydroxide (TPAOH, $C_{12}H_{29}NO$, 25 wt% in H_2O, Kente Catalysts Inc.), Aluminum isopropoxide (AIP, $C_9H_{21}AlO_3$, ≥99.9% metals basis, Shanghai Aladdin Biochemical Technology Co., Ltd), Deionized water (H_2O, Watsons), Deuterium oxide (D_2O, ≥99.9 atom% D, Shanghai Aladdin Biochemical Technology Co., Ltd), Ethanol (EtOH, C_2H_6O, ≥99.7%, Sinopharm Chemical Reagent Co., Ltd), Isopropanol (IPA, C_3H_8O, ≥99.7%, Sinopharm Chemical Reagent Co., Ltd), Dialysis tube (Spectra Por 3, Spectrum Laboratories), 1,3,5-triisopropylbenzene (TIPB, $C_{15}H_{24}$, ≥95%, Shanghai Aladdin Biochemical Technology Co., Ltd), 2,6-di-*tert*-butylpyridine (DTBPy, $C_{13}H_{21}N$, >97.0%, Shanghai Aladdin Biochemical Technology Co., Ltd), Commercial HZSM-5 zeolite (NKF-5, Si/Al molar ratio = 200, Nankai University Catalyst Co., Ltd).

2.2. Synthesis procedures

ZSM-5 zeolite with surface Si-Zoning was prepared under microwave heating starting from an aqueous clear sol with the molar composition 1 SiO_2: 0.36 TPAOH: 0.0025 Al_2O_3: 12.20 H_2O: 4 ethanol. Briefly, 0.017 g of AIP was added to 3.472 g of TEOS, and the resulting mixture was stirred at room temperature overnight. Finally, 4.881 g of TPAOH solution was added. The obtained mixture was rapidly stirred at room temperature for 24 h to ensure complete hydrolysis, then transferred into a 30 mL explosion-proof glass tube for a two-step heating process. Firstly, the solution was heated at 90 °C for 90 min under microwave irradiation, where the beginning time was defined as −90 min. Secondly, the obtained clear liquid was immediately heated at 130 °C for 6 h. After cooling to room temperature, a certain amount of ethanol was added into the slurry to reach an ethanol/Si molar ratio of 10. The suspension was stirred at room temperature for 2 h, followed by further microwave heating at 160 °C for 30 min. Finally, a certain amount of secondary silicate solution, with a molar composition of 0.5 SiO_2: 0.39 TPAOH: 10 ethanol: 13.21 H_2O, was further introduced into the cooled slurry. The resultant mixture was stirred at room temperature for 2 h and subsequently heated at 140 °C for 2 h under microwave irradiation. The solid product was collected by centrifugation at 10 000 rpm for 10 min, redispersed and washed three times with deionized water. And the collected solid was freeze-dried in vacuum at −50 °C and then calcined at 550 °C for further analysis. The sample was designated as Z5-200-Si, where 200 represents the initial Si/Al ratio, and Si indicates the additional silica added in the secondary step. Furthermore, to differentiate samples with different secondary silica loadings, the notation Z5-200-*k*Si was used, where *k* refers to the molar ratio of post-added silica to the silica in initial sol, varied between 0.3 to 1.1. No extra silica-added sample was named as Z5-200.

For the system with an initial Si/Al ratio of 100, the corresponding sample Z5-100 were obtained using an initial heating at 90 °C for 90 min and a secondary heating at 150 °C for 6 hours. All other procedural parameters were maintained consistent with those described above.

For the isopropanol-mediated synthesis, isopropanol (IPA) was used as an alternative alcohol. Prior to hydrothermal

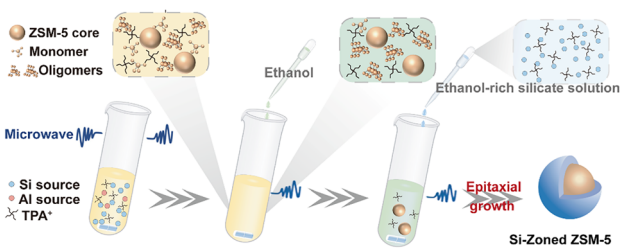

Scheme 1 Schematic illustration of the ethanol-mediated one-pot synthesis of Si-zoned ZSM-5 zeolites.

treatment, the ethanol generated from TEOS hydrolysis in both the initial system and the secondary silicon source was removed by rotary evaporation at 35 °C, and an equimolar amount of IPA was subsequently added. All other conditions remained unchanged.

2.3. Characterization

The Malvern Zetasizer Nano-ZS dynamic light scattering (DLS) instrument was employed to measure the particle size change during MFI zeolite synthesis. A certain amount of solution was taken from the explosion-proof glass tube at different heating time and was dilute and disperse with deionized water for DLS test. Every test at least 10 times and the average of the 6 test results was taken as accurate date. The morphologies and surface features of the samples were monitored by FEG S-4800 field emission scanning electron microscope. The structure features of the samples were visualized by JEM-F200 Transmission electron microscope. Powder X-ray diffraction (XRD) experiments were conducted with a Bruker D2 diffractometer (Cu-Kα, 10 kV, 30 mA) from 5 to 50°. Thermogravimetric measurements were performed on a SDT Q600 (TA) from 50 to 800 °C at a heating rate of 10 °C min^{-1} under a flow (100 mL min^{-1}) of high purity air. The Quantachrome iQ-2 physical adsorption instrument was used to acquire the adsorption isotherms and pore size distributions by Ar-sorption experiments at 87 K after outgassing at 573 K for 7 h, and textural parameters were calculated by Brunauer–Emmett–Teller (BET) method and *t*-plot method. The pore size distributions were also calculated by NLDFT method. All liquid ^{29}Si nuclear magnetic resonance (NMR) spectra were obtained on a Bruker AVANCE III HD 500 MHz spectrometer. An appropriate amount of the supernatant (0.6–0.8 mL) was transferred into 5 mm NMR quartz tube with a modified background-free commercial probe, and a small amount of D_2O was added in the tube for a lock signal. A solution tetramethylsilane (TMS) of in $CDCl_3$ as an external reference showed that the monomer resonance was at −71.9 ppm relative to TMS, which was then used as an internal reference. The relative amount of Q^n in oligomer fraction was calculated by decomposing the ^{29}Si NMR spectra.

The acidic properties of samples were obtained by temperature-programmed desorption of ammonia (NH_3-TPD) performed on the Micromeritics 2920 chemisorption analyzer. The analysis of the externally accessible Brønsted acid sites was completed by using the Bruker Invenio S instrument Fourier-transform infrared spectrometer to collect 2,6-di-*tert*-butylpyridine infrared (DTBPy-IR) spectra. Self-supported wafer of sample was places in the IR cell and evacuated at 450 °C for 75 min with a vacuum system. Reference spectra at 200 °C were recorded. Prior to collecting the DTBPy-IR spectra, the outgassed samples were placed in 2,6-di-*tert*-butylpyridine vapor at room temperature for 15 min. The DTBPy-IR spectra were collected after outgassed 2,6-di-*tert*-butylpyridine at 200 °C in a vacuum environment for 30 min. The element content and ratios in the products were analysed by inductively coupled plasma-atomic emission spectrometry (ICP) on a PE-8000 spectrometer. X-ray photoelectron spectroscopy (XPS) experiments were conducted on a Thermo Fisher Scientific K-Alpha (Al-Kα) to analyze the surface Si/Al ratio of the zeolite.

To assess the absence of Brønsted acid site on external surface, 1,3,5-triisopropylbenzene (TIPB) cracking over the various zeolite products was conducted in a tandem μ reactor (Frontier lab, Rx-3050TR). Typically, 60 mg of catalyst was loaded into a quartz tube μ-reactor and activated by N_2 with a flow rate of 45 mL min^{-1} at 550 °C for 2 h. TIPB was then introduced into the reaction system through pulse injection, with each injection being 0.40 μL at 450 °C. The products were analyzed online using a Shimadzu GC-2030 chromatograph equipped with a hydrogen ion flame detector (FID) and HP-5 capillary column. The main products were benzene, diisopropylbenzene (DIPB) and isopropylbenzene (IPB) and the conversion was calculated using the following equation:

$$\text{Conversion}(\%) = 1 - \frac{\text{moles of residual TIPB}}{\text{moles of (residual TIPB} + \text{DIPB} + \text{IPB} + \text{benzene)}}$$

3. Results and discussion

3.1. Synthesis and structural characterization of surface Si-zoned ZSM-5

ZSM-5 zeolite with a Si-enriched surface was synthesized *via* an ethanol-enabled one-pot, two-step strategy. In the first step, ZSM-5 zeolite cores with different initial Si/Al ratios were synthesized under ethanol-assisted conditions. Subsequently, a controlled amount of hydrolyzed pure-silica solution was introduced into the same synthesis system, followed by further thermal treatment to grow the silica-rich shell. The resulting zeolites are denoted as Z5-*x*-*k*Si, where *x* refers to the Si/Al ratio of the initial synthesis gel and *k* represents the molar ratio of post-added silica to the silica in the initial sol. In addition, a commercial HZSM-5 zeolite (Com-ZSM-5, Si/Al = 200) was used as a reference material for structural and catalytic comparison.

The elemental composition of the bulk and surface was quantified by inductively coupled plasma atomic emission spectroscopy (ICP-AES) and X-ray photoelectron spectroscopy (XPS). As summarized in Table 1, the surface Si/Al ratios of both Z5-200-1.1Si and Z5-100-1.0Si tend to ∞, much higher than their corresponding bulk values, indicating a pronounced Si enrichment at the outer region. Consistently, the Al 2p signal is

Table 1 The Si/Al ratios and textural properties of Z5-*x*-*k*Si samples

Sample	Si/Al ratio (ICP-AES)	Si/Al ratio (XPS)	Surface area (m^2 g^{-1})			Pore volume (cm^3 g^{-1})	
			S_{BET} [a]	S_{micro} [b]	S_{ext} [b]	V_{total} [c]	V_{micro} [b]
Z5-200-1.1Si	327	∞	550	413	137	0.36	0.16
Z5-100-1.0Si	189	∞	517	387	130	0.33	0.16

[a] Determined by the multi-point BET method. [b] Analyzed by *t*-plot method. [c] Using the adsorption data at P/P_0 = 0.974.

nearly absent in the XPS spectra (Fig. 1a), demonstrating that aluminum species from the initial synthesis gel are almost completely incorporated into the zeolite cores and do not significantly enter the subsequently grown shell. This decoupling of bulk and surface composition is particularly noteworthy given the one-pot nature of the synthesis, and confirms that this synthesis strategy indeed enables a clean, aluminum-free environment for the secondary silica deposition.

The integrity and catalytic inertness of the silica-rich shell were further assessed using two complementary bulky probe molecules, 2,6-di-*tert*-butylpyridine (DTBPy) and 1,3,5-triisopropylbenzene (TIPB), both of which are too large to enter the micropores of ZSM-5 and thus probe only Brønsted acid sites located at or near the external surface.[30–32] Compared with Com-ZSM-5 with similar bulk Si/Al ratio, the characteristic 1616 cm^{-1} band in the DTBPy-IR spectra almost completely disappears for Z5-*x*-*k*Si (Fig. 1b), indicating effective blocking or removal of external Brønsted acid sites. In line with this observation, the TIPB cracking activity is drastically suppressed under identical conditions (Fig. 1c). The convergence of these two independent probe reactions demonstrates that the silica-rich shell formed in the one-pot route is not only structurally continuous but also catalytically inert toward bulky reactants. In addition, NH_3-TPD measurements show that the acid strength remains essentially unchanged, whereas the total acidity decreases after shell growth (Fig. S1 and Table S1), consistent with dilution of acid sites by the silica-rich shell.

The crystallinity and textural properties of the shell-coated ZSM-5 are preserved during the secondary growth step. Powder X-ray diffraction (PXRD) patterns of the Z5-200-1.1Si and Z5-100-1.0Si (Fig. 1d) display only the diffraction characteristic of the MFI framework, with no additional peaks attributable to amorphous silica (20–30° in 2θ) or other crystalline impurities. Argon adsorption–desorption isotherms (Fig. 1e) exhibit typical type I adsorption behavior, characteristic of purely microporous materials. The BET surface areas and micropore volumes are

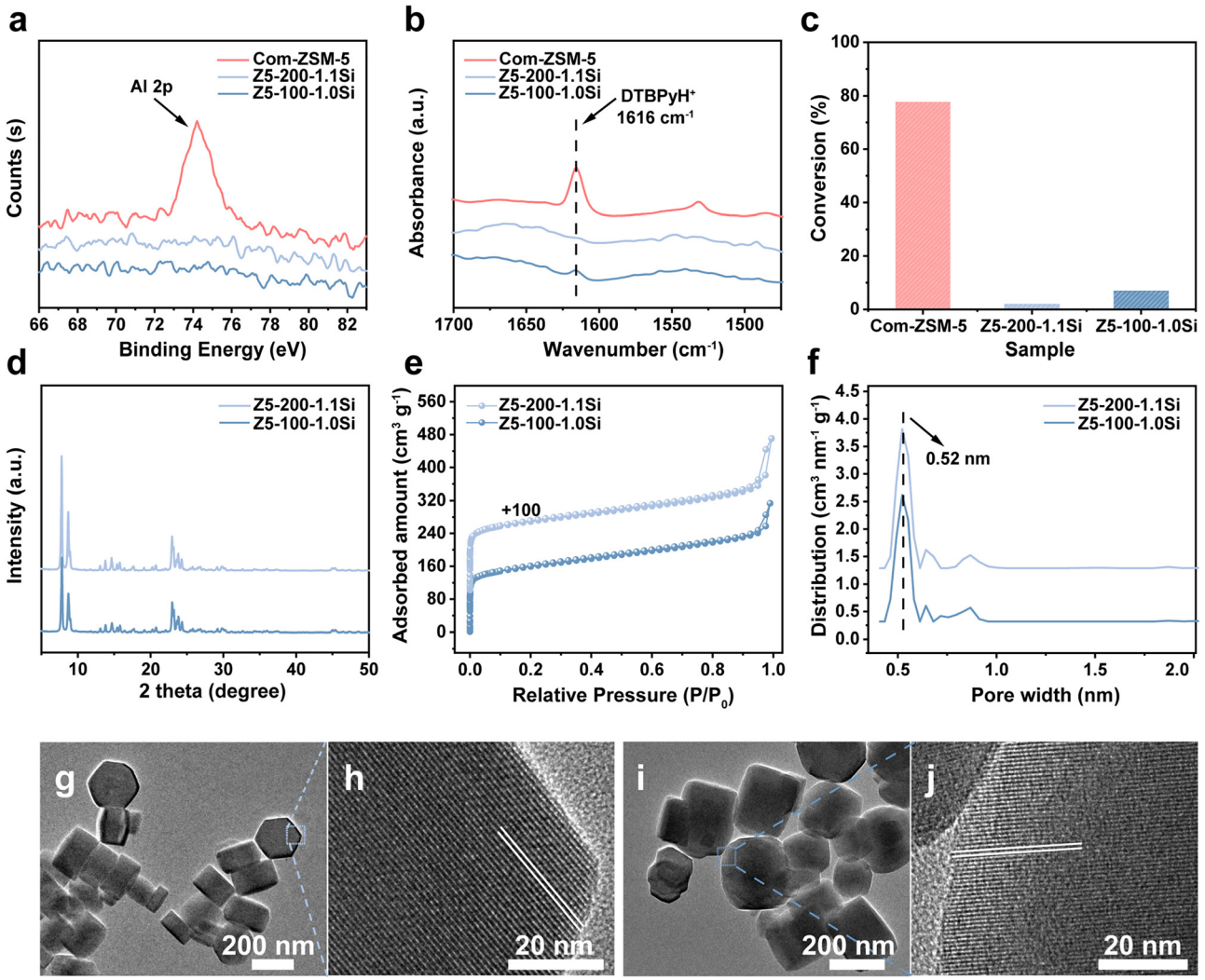

Fig. 1 Characterization results of the Z5-*x*-*k*Si and commercial ZSM-5 zeolites: (a) Al 2p XPS spectra; (b) *in situ* FT-IR spectra of DTBPy adsorption at 200 °C; (c) catalytic TIPB cracking over ZSM-5 samples at 450 °C; (d) XRD patterns; (e) Ar adsorption–desorption isotherms at 87 K and (f) pore size distributions calculated by NLDFT and TEM images of (g) and (h) Z5-200-1.1Si and (i) and (j) Z5-100-1.0Si.

comparable to those of conventional MFI zeolites reported in the literature (Table 1),[33,34] and the pore size distribution reveals a dominant micropore centered at 0.52 nm (Fig. 1f), corresponding to the intrinsic MFI channel system and confirming accessible and well-connected microporous channels.[35,36] High-resolution transmission electron microscopy (HRTEM) images further reveal well-resolved lattice fringes throughout the entire crystals (Fig. 1g–j), demonstrating a fully crystalline and structurally continuous MFI framework. Thermogravimetric analysis (TGA) provides supplementary evidence consistent with the thermal decomposition behavior of typical TPA-containing ZSM-5 materials (Fig. S2). Taken together, these results confirm that the one-pot, two-step strategy successfully produces ZSM-5 zeolites with a Si-enriched, catalytically inert surface shell while maintaining high crystallinity and microporosity in the entire MFI framework.

3.2. Thickness control of the silicon-rich shell in surface Si-zoned ZSM-5

Siliceous zeolite layers surrounding an acidic zeolite core, beyond passivating external acid sites, are known to modulate molecular diffusion by extending the effective diffusion path length of reactants, thereby enhancing diffusion-controlled product shape selectivity.[37,38] Nevertheless, excessive shell growth may introduce undesirable diffusion limitations and reduce catalytic accessibility,[39] highlighting the importance of precisely controlling shell thickness. Traditionally, shell thickness has been controlled either kinetically, by quenching hydrothermal growth at a predetermined time,[17] or thermodynamically, by adjusting the total silica content to reach equilibrium incorporation.[40] Since kinetic control can lead to incomplete utilization of the silica source and potentially lead to amorphous deposition, in this work we tune the shell thickness by varying the amount of secondary silica added. The system with an initial Si/Al ratio of 200 was selected for detailed investigation.

Dynamic light scattering (DLS) measurements reveal a steady, monotonic increase in particle size with increasing levels of secondary silicate addition (Table S2). Notably, the dependence of the shell thickness on the amount added can be well described by the following equation (Fig. 2a and Table S2):

$$T = d \times \frac{\sqrt[3]{1+k} - 1}{2} \quad (1)$$

The parameter d represents the average diameter of the parent Z5-200 cores and k is the molar ratio of post-added silica (as SiO_2) to the silica in the initial sol. T is the shell thickness of the final Z5-200-kSi particles. As detailed in the Supporting Information, the derivation of this relation is based on three key assumptions: (i) the initial silica source is completely incorporated into the ZSM-5 cores, (ii) no homogeneous nucleation occurs during pure-silica shell formation, and (iii) the secondarily added silica is nearly completely consumed in the growth of the shell. The excellent agreement between the experimentally obtained thicknesses and those predicted from eqn (1) indicates that these conditions are essentially fulfilled in our ethanol-assisted one-pot system (Fig. 2a).

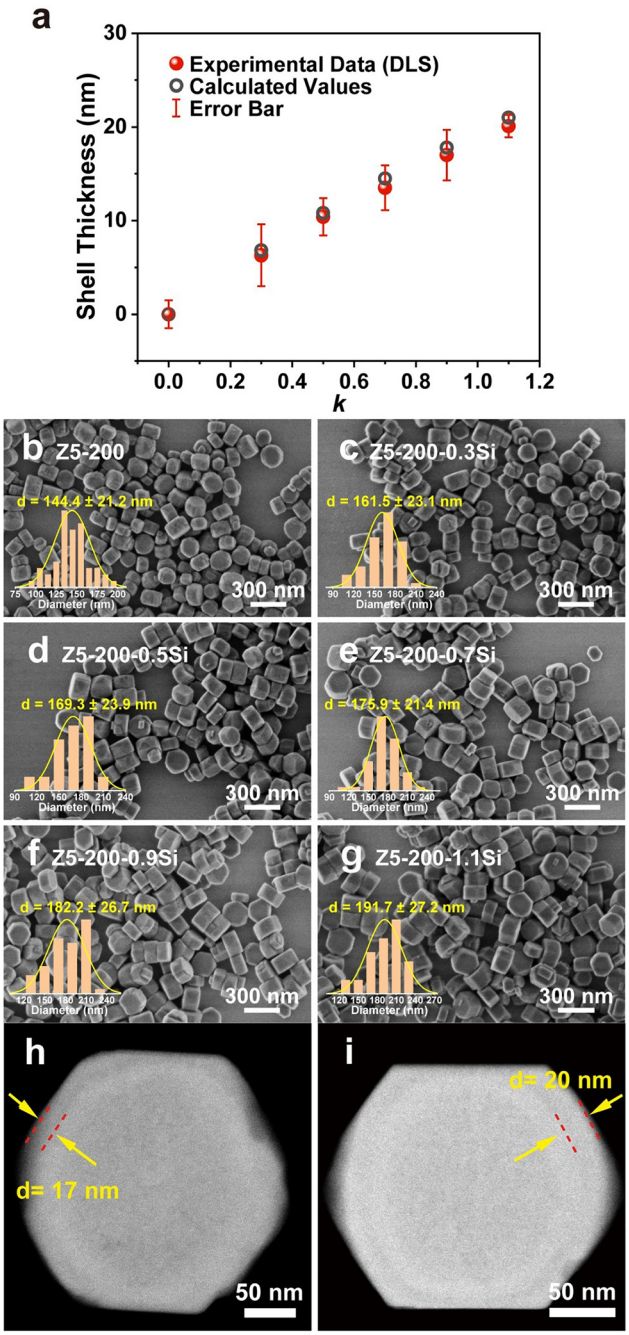

Fig. 2 (a) Comparison between experimentally measured and calculated shell thicknesses of ZSM-5 at different k values. Filled red symbols represent thicknesses determined by DLS measurements, while open symbols denote calculated values. Error bars indicate the standard deviation of the DLS measurements (n = 6); (b)–(g) SEM images of Z5-200 and Z5-200-kSi samples (Insets: Size distribution of samples in the visual field); (h) and (i) HAADF-STEM images of (h) Z5-200-0.9Si and (i) Z5-200-1.1Si.

Morphological analysis further supports this conclusion. As shown in Fig. 2b–g, the particles evolve toward more regular, well-defined morphologies as the silica addition increases, and the size distributions derived from scanning electron

microscopy (SEM) are in good agreement with the DLS results (Table S2). Moreover, when the silica addition reaches a sufficient level, a silica-rich overlayer can be directly visualized in High-angle annular dark-field STEM (HAADF-STEM) images (Fig. 2h, i and Fig. S3). For example, in the Z5-200-1.1Si sample, the HAADF image reveals a silica-rich overlayer with an estimated thickness of approximately 20 nm (Fig. 2i), in good agreement with the theoretically calculated value (Fig. 2a and Table S2). This quantitative consistency between calculated and observed shell thickness, together with the monotonic particle-size evolution, demonstrate that the prerequisite condition is fulfilled, namely the absence of homogeneous nucleation and the high utilization efficiency of both the initial and post-added silica sources.

HRTEM images show continuous lattice fringes across all zeolite samples with varying shell thicknesses. The alignment of lattice orientations between the outer shell and the crystal core (Fig. S4) confirms that the post-added silicate species are incorporated into zeolite core *via* epitaxial growth. The external surface acidity was further investigated for samples with systematically tuned shell thicknesses employing the same surface-sensitive probes described above. As shown in Fig. S5, even when the post-added silica level is reduced from $k = 1.1$ to 0.3, the external surfaces consistently remain acid-passivated and catalytically inert toward bulky reactants. Notably, even at the lowest post-added silica level ($k = 0.3$), corresponding to a shell thickness of approximately 7 nm, complete surface coverage is still achieved, highlighting a key advantage of the present approach, namely its ability to enable uniform deposition of post-added silica across the entire crystal surface. This behavior benefits from a classical layer-by-layer growth mode, as further substantiated in the following section. Overall, the thickness of the silica-rich shell in surface Si-zoned ZSM-5 can be precisely controlled by adjusting the amount of secondary pure-silica solution introduced into the system. The geometric correlation between silica dosage, particle size, and shell thickness provides an independent verification of the ethanol-enabled one-pot, two-step strategy.

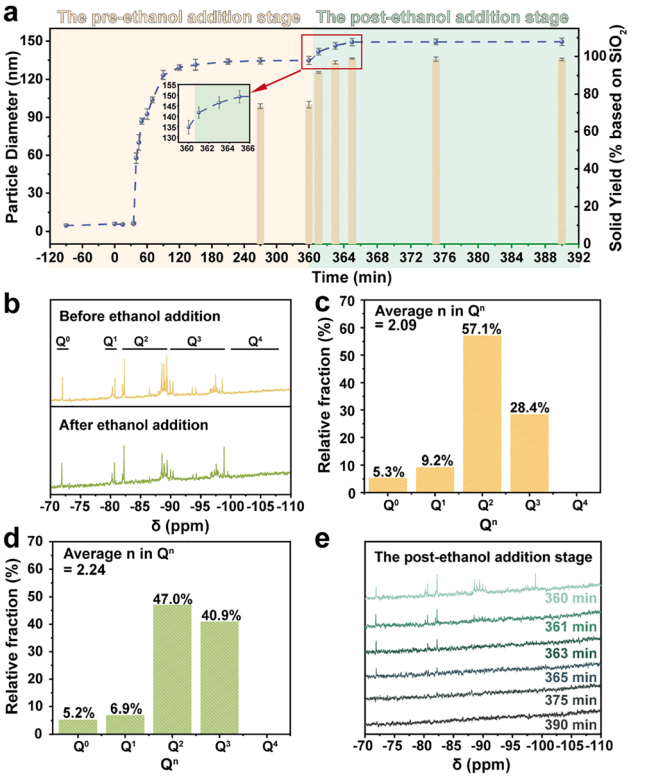

Fig. 3 (a) Particle size evolution of the precursor suspension and solid yield during hydrothermal treatment in the synthesis system with an initial Si/Al ratio of 200. The curves represent particle diameters and the bar charts show the solid yields obtained by centrifugation after removing the structure-directing agent *via* calcination at 550 °C. Error bars indicate the standard deviation (SD). The data for particle size are presented as the mean ± SD ($n = 6$), and those for yield are presented as the mean ± SD ($n = 4$); (b) ^{29}Si NMR spectra of the supernatants were obtained by centrifugation at 360 min before and after the addition of ethanol (without further heating) and the oligomer Q^n ranges are indicated, and Q^n distribution of oligomers determined with liquid-state ^{29}Si NMR spectroscopic analysis and average connectivity n of the Q^n-type silicon atoms in the oligomers (c) before and (d) after ethanol addition (without further heating); (e) ^{29}Si NMR spectra of the supernatants obtained by centrifugation at different crystallization times during the post-ethanol addition stage.

3.3. Role of ethanol in one-pot construction of surface Si-zoned ZSM-5

3.3.1. Role of ethanol in core formation. Ethanol as a co-solvent can substantially modify the solvation environment and enhance the reactivity of silicate-aluminate species.[41–43] However, previous studies,[44,45] including our own work,[29] have shown that the presence of ethanol prolongs the nucleation period and significantly slows down the subsequent crystal growth, particularly during the rapid particle-attachment stage associated with nonclassical crystallization. To avoid these kinetic disadvantages while still exploiting the beneficial effect of ethanol, we adopted a post-addition strategy in which ethanol was introduced only after the completion of the initial crystallization stage, followed by further thermal treatment.

The synthetic procedure of core ZSM-5 was monitored by dynamic light scattering (DLS) measurement, which provides a quasi *in situ* characterization of particle size evolution in the mother liquor, with no post-treatment such as centrifugation or washing performed prior to analysis except for necessary dilution, and thus reflect the crystallization progress of the system. As shown in Fig. 3a, prior to ethanol addition (yellow region), the crystallization process displayed a typical S-shaped curve, which could be easily divided into nucleation and crystal growth stages, separated by an ''inflection point''. Upon reaching the inflection point (35 min), a rapid increase in particle size was observed, accompanied by the visible change from a colorless, transparent solution to a milky suspension (Fig. S6) and the formation of centrifugable crystalline ZSM-5 zeolites (Fig. S7), with sizes matching DLS results (Fig. S8). Finally, the average particle size stabilized at approximately 135 nm, and the centrifugation yield plateaued at about 74%. After ethanol addition, however, further heating led to an additional increase in particle size and centrifugation yield (Fig. 3a). As summarized in Table S3, the practically complete yield indicates nearly

full utilization of reactive species, which is also observed in systems with higher Al content. These results show that ethanol facilitates further crystal growth rather than nucleation of new nuclei and drives the system toward a clean, species-depleted mother liquor that provides an ideal environment for the subsequent pure-silica shell growth.

To clarify how ethanol promotes this additional crystallization, liquid-state ^{29}Si nuclear magnetic resonance (NMR) was employed to identify types and distribution of silica species in the supernatant obtained by centrifugation before and after ethanol addition. Generally, broad signals arise from nanoparticles whereas narrow resonances correspond to dissolved monomeric and oligomeric silicate species.[46–48] As shown in Fig. 3b, only sharp singlets are observed in the ^{29}Si NMR spectra of the supernatant, both before and after ethanol addition (without further heating), suggesting that particulate Si species are essentially absent from the liquid phase. To independently confirm the depletion of particulate species, we compared the solid yields obtained by centrifugation and by dialysis (Table S4). Because dialysis selectively removes soluble species while retaining zeolite crystals and ultra-small particles that cannot be retained during centrifugation (such as nuclei), the solid yield obtained by dialysis reflects the total amount of particulate species in the system.[49] The good agreement between the yields determined by dialysis and by centrifugation therefore corroborates that the liquid phase contains predominantly soluble silicate species, in line with the NMR analysis. Besides, the spectral regions assigned to Q^n environments in Fig. 3b are consistent with the existing literature reports on silicate speciation.[46–48,50] Notably, quantitative analysis of the ^{29}Si NMR spectra (Fig. 3c, 3d) reveals that, upon ethanol addition at room temperature, the percentage of silicon in Q^0, Q^1 and Q^2 environments decreases, while the Q^3 contribution increases, leading to a higher average connectivity of silicon atoms in the soluble silicate species. As heating proceeds in the presence of ethanol, both the intensity and number of these sharp resonance peaks markedly diminish (Fig. 3e), which is attributed to the progressive incorporation of these soluble silica species into the solid zeolite phase, in agreement with the observed increase in centrifugation yield (Fig. 3a). Taken together, these observations indicate that ethanol perturbs the intrinsic speciation of dissolved silicate oligomers, shifting the dissolution–condensation equilibrium toward more highly connected species that are more readily incorporated at the crystal–solution interface and thereby generating a clean, Al-depleted mother liquor. This ''clean'' liquid phase is a prerequisite for the subsequent pure-silica shell growth and is thus central to the success of the ethanol-enabled one-pot construction of surface Si zoning.

3.3.2. Role of ethanol in shell growth. Introduction of a secondary silica source is required to construct the silica-rich outer shell. The speciation and composition of this silica source are crucial: an inappropriate speciation or composition may promote homogeneous nucleation or non-uniform deposition,[51,52] thereby compromising controlled and conformal shell growth. Guided by the results in Section 3.3.1, we prepared an ethanol-rich pure-silica solution whose composition mimics that of the ethanol-containing supernatant obtained after core formation, characterized by a high alkali-to-silicon ratio and a high ethanol content. This feed is hereafter referred to as the ethanol-rich silicate solution.

As shown in Fig. 4a, decreasing the OH^-/Si molar ratio of the ethanol-rich silicate solution leads to broad ^{29}Si NMR signals indicative of particulate silicate species. Dialysis experiments corroborate this observation: the ethanol-rich silicate solution gives negligible solid residue ($<1\%$), whereas the solution with a reduced OH^-/Si ratio yields about 40% solid recovery (Table S5). These results unequivocally demonstrate that particulate species are essentially absent in the ethanol-rich silicate solution but are abundant when the OH^-/Si ratio is reduced. Such particulate silicate species are undesirable, as they readily act as precursors for homogeneous nucleation and promote uncontrolled crystal growth. Moreover, their incorporation also disrupts uniform shell formation and leads to the rough surface morphologies depicted in Fig. S9.

We further examined the role of ethanol by lowering only the ethanol content of the silicate feed while keeping the OH^-/Si ratio comparable. In the low-ethanol silicate solution (ethanol originating solely from TEOS hydrolysis), the silicate species still appear predominantly as monomeric and oligomeric forms, as evidenced by the presence of sharp ^{29}Si NMR singlets and the near-zero solid recovery upon dialysis (Fig. 4a and Table S5). However, quantitative analysis shows that the average silicate connectivity is significantly reduced relative to the ethanol-rich silicate solution (Fig. 4b and c), consistent with the conclusion that ethanol promotes the formation of more highly connected soluble silicate species. When both silicate solutions were subjected to hydrothermal treatment at 140 °C for 2–8 h, only the ethanol-rich silicate solution crystallized to form zeolite after 3 h (Fig. S10a and c), with a final centrifugation-derived solid yield exceeding 90%. In contrast, the low-ethanol silicate solution remained clear and transparent throughout (Fig. S10b), indicating no crystallization occurred. These results further substantiate ethanol's critical role in promoting zeolite crystallization from highly connected, yet still soluble silicate oligomers.

When the ethanol-rich silicate solution is added to the Z5-200 core suspension and heated at 140 °C, the added silica is consumed within only 2 h, corresponding to a markedly high utilization rate that is substantially faster than that observed for independent crystallization of the same solution (Fig. S10a). This accelerated consumption in the presence of pre-existing crystals indicates that, under ethanol-mediated conditions, these highly connected yet still soluble silicate species preferentially undergo classical addition onto existing zeolite surfaces rather than following the more energetically demanding pathway of *de novo* nucleation followed by growth.[53] Owing to this ethanol-assisted layer-by-layer classical growth mode, the secondary silica source is efficiently utilized, allowing for precise control over the shell thickness by varying the amount of added silicate, as demonstrated for the Z5-200-*k*Si series (Fig. 2 and Fig. S3, S4). Furthermore, SEM images (Fig. 4d–g) directly

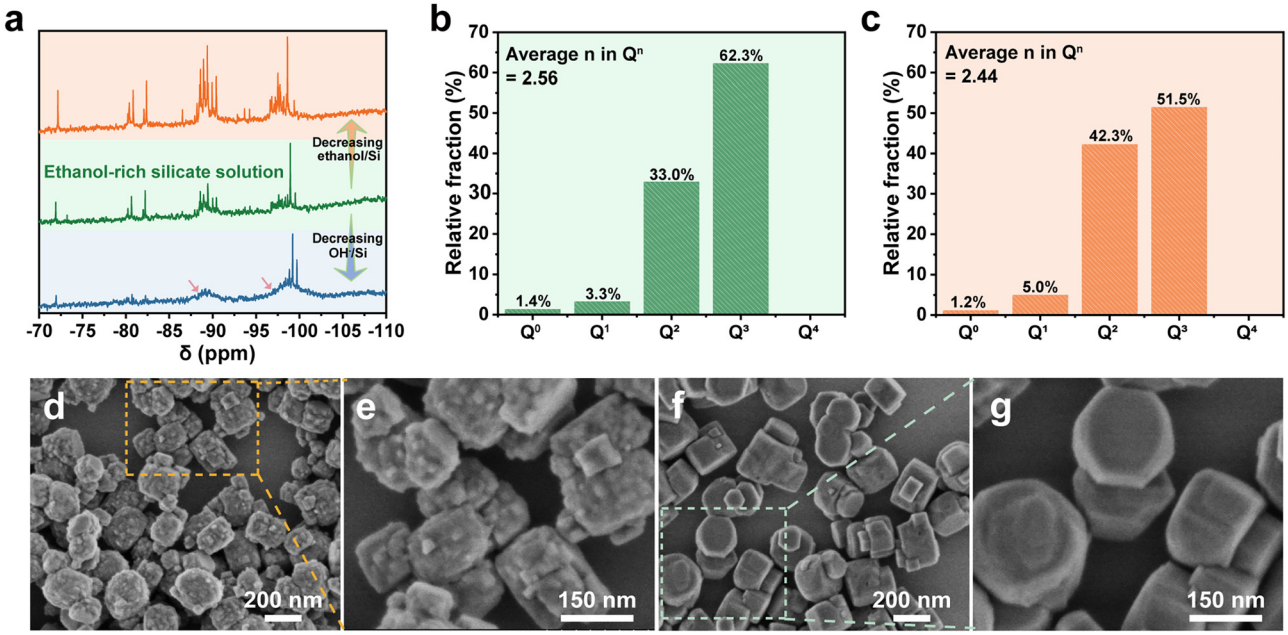

Fig. 4 (a) Liquid-state ^{29}Si NMR spectra of the silicalite-1 aging sol with different initial compositions. The pink arrows indicate the position of the broad particle bands; (b) and (c) Q^n distribution of oligomers determined by liquid-state ^{29}Si NMR spectroscopy, and the average connectivity (n) of Q^n-type silicon atoms in the oligomers of (b) the ethanol-rich silicate solution and (c) the solution with reduced ethanol/Si molar ratio and (d)–(g) SEM images of Z5-100 (d) and (e) and Z5-100-1.0Si (f) and (g).

contrast the Z5-100 cores and the corresponding Z5-100-1.0Si products. The initially rough and irregular core surfaces are converted into smooth, continuous shells after shell growth, illustrating that the ethanol-assisted strategy can uniformly coat even morphologically non-ideal cores.

To examine whether the present strategy is specific to ethanol, isopropanol (IPA) was also tested as an alternative alcohol under otherwise comparable conditions after removal of ethanol generated from TEOS hydrolysis. The resulting samples still exhibited the MFI framework and showed smoother particle surfaces after secondary silica addition (Fig. S11), indicating that shell growth can also occur in the IPA-assisted system. However, the decrease in the DTBPy-IR signal and the suppression of TIPB cracking were less pronounced than in the ethanol-assisted case, suggesting weaker external acid-site passivation under the present conditions. Considering that establishment of the IPA-assisted system required an additional ethanol-removal step, which may alter the liquid-phase silicate/aluminate speciation, these results indicate that the present strategy is not uniquely limited to ethanol and further support the mechanistic picture proposed here, namely that alcohol-mediated modulation of liquid-phase species facilitates efficient species incorporation and subsequent silica-shell growth.

In summary, ethanol plays a critical role in the one-pot synthesis of surface Si-zoned ZSM-5 zeolites with tunable shell thickness. In the core-formation stage, ethanol enables near-quantitative utilization of aluminosilicate species, thereby creating an Al-depleted mother liquor that is ideally suited for subsequent pure-silica shell growth. In the shell-growth stage, ethanol modifies the speciation of dissolved silicate oligomers, shifting the dissolution-condensation equilibrium toward more highly polymerized yet soluble species that are readily incorporated *via* classical monomer/oligomer addition at the crystal-solution interface. This classical addition pathway under ethanol-rich conditions ensures uniform deposition of soluble silicate species across the entire crystalline surface, including regions of high curvature or geometric confinement, thereby enabling controlled construction of a smooth, silica-rich shell without homogeneous nucleation.

4. Conclusion

To sum up, we have developed an ethanol-assisted one-pot, two-step strategy for synthesizing surface Si-zoned ZSM-5 zeolites with tunable shell thickness. Ethanol promotes a classical crystallization pathway and enables near-complete utilization of aluminosilicate species in the core-formation stage, generating an Al-depleted mother liquor suitable for subsequent pure-silica shell growth. Upon addition of an ethanol-rich silicate feed to the same system, soluble silicate species are incorporated *via* a classical layer-by-layer growth mode to form a silica-rich shell with tunable thickness, yielding ZSM-5 zeolites with well-defined surface Si zoning. Bulk and surface analyses, complemented by DTBPy-IR spectroscopy and TIPB cracking tests, confirm that the outer shell is silica-rich, structurally continuous, and effectively inert toward bulky reactants. Overall, this ethanol-enabled one-pot strategy provides a high-yield and compositionally efficient route to surface Si-zoned ZSM-5

and offers a versatile platform for tailoring external surface properties in zeolite-based catalysis.

Author contributions

The manuscript was written through contributions of all authors. All authors contributed extensively to the work presented in this paper. Jiayu Yu carried out the methodology, investigation, data curation, formal analysis, and writing-original draft. Di Pan participated in data curation and analysis. Ke Du performed the methodology and investigation. Wei Chen participated in the investigation. Jian Zhou directed the catalytic and characterization research and contributed to the preparation and writing of the manuscript. Yi Tang participated in the analysis and discussion of the experimental results. Yahong Zhang designed and directed the research, as well as contributed to the preparation and writing of the manuscript.

Conflicts of interest

There are no conflicts to declare.

Data availability

The data supporting this article have been included as part of the supplementary information (SI). Supplementary information provides additional details on shell thickness calculations and experimental procedures; PXRD, SEM, TEM, DLS, optical photographs, DTBPy-IR, NH_3-TPD, and catalytic TIPB cracking results for the samples. See DOI: **https://doi.org/10.1039/d6qm00097e**.

Acknowledgements

The authors gratefully acknowledge the financial support from the National Key R&D Program of China (2023YFA1507602), National Natural Science Foundation of China (22472037, U24A20488, 22293023) and the Science and Technology Commission of Shanghai Municipality (2024ZDSYS02).

Notes and references

1 J. Shi, Y. Wang, W. Yang, Y. Tang and Z. Xie, Recent advances of pore system construction in zeolite-catalyzed chemical industry processes, *Chem. Soc. Rev.*, 2015, **44**, 8877–8903.

2 B. Bensafi, N. Chouat and F. Djafri, The universal zeolite ZSM-5: Structure and synthesis strategies. A review, *Coord. Chem. Rev.*, 2023, **496**, 215397.

3 L. Lakiss, F. Ngoye, C. Canaff, S. Laforge, Y. Pouilloux, Z. Qin, M. Tarighi, K. Thomas, V. Valtchev, A. Vicente, L. Pinard, J.-P. Gilson and C. Fernandez, On the remarkable resistance to coke formation of nanometer-sized and hierarchical MFI zeolites during ethanol to hydrocarbons transformation, *J. Catal.*, 2015, **328**, 165–172.

4 T. T. Le, A. Chawla and J. D. Rimer, Impact of acid site speciation and spatial gradients on zeolite catalysis, *J. Catal.*, 2020, **391**, 56–68.

5 T. T. Le, W. Qin, A. Agarwal, N. Nikolopoulos, D. Fu, M. D. Patton, C. Weiland, S. R. Bare, J. C. Palmer, B. M. Weckhuysen and J. D. Rimer, Elemental zoning enhances mass transport in zeolite catalysts for methanol to hydrocarbons, *Nat. Catal.*, 2023, **6**, 254–265.

6 J. C. Groen, T. Bach, U. Ziese, A. M. Paulaime-van Donk, K. P. de Jong, J. A. Moulijn and J. Pérez-Ramírez, Creation of Hollow Zeolite Architectures by Controlled Desilication of Al-Zoned ZSM-5 Crystals, *J. Am. Chem. Soc.*, 2005, **127**, 10792–10793.

7 Y. Shen, Z. Qin, S. Asahina, N. Asano, G. Zhang, S. Qian, Y. Ma, Z. Yan, X. Liu and S. Mintova, The inner heterogeneity of ZSM-5 zeolite crystals, *J. Mater. Chem. A*, 2021, **9**, 4203–4212.

8 K. Du, X. Zhang, T. He, W. Shen, H. Xu, Y. Tang, X.-M. Cao, Z. Huang and Y. Zhang, Dynamic Evolution of Structural Ordering and Aluminum Redistribution During ZSM-5 Zeolite Crystallization, *Angew. Chem., Int. Ed.*, 2025, **64**, e202507223.

9 S. Inagaki, S. Shinoda, Y. Kaneko, K. Takechi, R. Komatsu, Y. Tsuboi, H. Yamazaki, J. N. Kondo and Y. Kubota, Facile Fabrication of ZSM-5 Zeolite Catalyst with High Durability to Coke Formation during Catalytic Cracking of Paraffins, *ACS Catal.*, 2013, **3**, 74–78.

10 J.-H. Kim, A. Ishida, M. Okajima and M. Niwa, Modification of HZSM-5 by CVD of Various Silicon Compounds and Generation of Para-Selectivity, *J. Catal.*, 1996, **161**, 387–392.

11 S. Hu, J. Liu, J. Chen, J. Meng, G. Ye and X. Zhou, Reducing External Surface Diffusion Barriers by Chemical Vapor Deposition for Improved Zeolite Catalysis, *Ind. Eng. Chem. Res.*, 2022, **61**, 5747–5756.

12 Z. Zhu, Z. Xie, Q. Chen, D. Kong, W. Li, W. Yang and C. Li, Chemical liquid deposition with polysiloxane of ZSM-5 and its effect on acidity and catalytic properties, *Microporous Mesoporous Mater.*, 2007, **101**, 169–175.

13 Y. Fang, Z. Huang, S. Wang, H. Sheng, W. Hua, Y. Yue, W. Shen and H. Xu, Enhancing BTX selectivity of the syngas to aromatics reaction through silylation of CTAB pretreated ZSM-5, *Catal. Sci. Technol.*, 2021, **11**, 4944–4952.

14 S. Zheng, A. Jentys and J. A. Lercher, On the enhanced para-selectivity of HZSM-5 modified by antimony oxide, *J. Catal.*, 2003, **219**, 310–319.

15 W. Tan, M. Liu, Y. Zhao, K. Hou, H. Wu, A. Zhang, H. Liu, Y. Wang, C. Song and X. Guo, Para-selective methylation of toluene with methanol over nano-sized ZSM-5 catalysts: Synergistic effects of surface modifications with SiO_2, P_2O_5 and MgO, *Microporous Mesoporous Mater.*, 2014, **196**, 18–30.

16 B. Zhang, Z. Zhong, Q. Xie, P. Chen and R. Ruan, Reducing coke formation in the catalytic fast pyrolysis of bio-derived furan with surface modified HZSM-5 catalysts, *RSC Adv.*, 2015, **5**, 56286–56292.

17 A. Ghorbanpour, A. Gumidyala, L. C. Grabow, S. P. Crossley and J. D. Rimer, Epitaxial Growth of ZSM-5@Silicalite-1:

A Core–Shell Zeolite Designed with Passivated Surface Acidity, *ACS Nano*, 2015, **9**, 4006–4016.

18 G. Giordano, M. Migliori, G. Ferrarelli, G. Giorgianni, F. Dalena, P. Peng, M. Debost, P. Boullay, Z. Liu, H. Guo, Z.-F. Yan and S. Mintova, Passivated Surface of High Aluminum Containing ZSM-5 by Silicalite-1: Synthesis and Application in Dehydration Reaction, *ACS Sustainable Chem. Eng.*, 2022, **10**, 4839–4848.

19 N. Wang, J. Li, W. Sun, Y. Hou, L. Zhang, X. Hu, Y. Yang, X. Chen, C. Chen, B. Chen and W. Qian, Rational Design of Zinc/Zeolite Catalyst: Selective Formation of p-Xylene from Methanol to Aromatics Reaction, *Angew. Chem., Int. Ed.*, 2022, **61**, e202114786.

20 X. Cui, H. Lyu, Y. Chai, B. Liu, D. Zhao and C. Liu, Selective aromatization of 1-hexene to BTX over core-shell structured Silicalite-1@ZSM-5 catalyst, *Sep. Purif. Technol.*, 2024, **349**, 127881.

21 S. Zheng, H. R. Heydenrych, H. P. Röger, A. Jentys and J. A. Lercher, On the Enhanced Selectivity of HZSM-5 Modified by Chemical Liquid Deposition, *Top. Catal.*, 2003, **22**, 101–106.

22 P. Losch, M. Boltz, C. Bernardon, B. Louis, A. Palčić and V. Valtchev, Impact of external surface passivation of nano-ZSM-5 zeolites in the methanol-to-olefins reaction, *Appl. Catal., A*, 2016, **509**, 30–37.

23 G. Ferrarelli, M. Migliori and E. Catizzone, Recent Trends in Tailoring External Acidity in Zeolites for Catalysis, *ACS Omega*, 2024, **9**, 29072–29087.

24 K. Miyake, R. Inoue, T. Miura, M. Nakai, H. Al-Jabri, Y. Hirota, Y. Uchida, S. Tanaka, M. Miyamoto, S. Inagaki, Y. Kubota, C. Y. Kong and N. Nishiyama, Improving hydrothermal stability of acid sites in MFI type aluminosilicate zeolite (ZSM-5) by coating MFI type all silica zeolite (silicalite-1) shell layer, *Microporous Mesoporous Mater.*, 2019, **288**, 109523.

25 T. Wang, Y. Xu, C. Shi, F. Jiang, B. Liu and X. Liu, Direct production of aromatics from syngas over a hybrid FeMn Fischer–Tropsch catalyst and HZSM-5 zeolite: local environment effect and mechanism-directed tuning of the aromatic selectivity, *Catal. Sci. Technol.*, 2019, **9**, 3933–3946.

26 Q. Wu, L. Zhu, Y. Chu, X. Liu, C. Zhang, J. Zhang, H. Xu, J. Xu, F. Deng, Z. Feng, X. Meng and F.-S. Xiao, Sustainable Synthesis of Pure Silica Zeolites from a Combined Strategy of Zeolite Seeding and Alcohol Filling, *Angew. Chem., Int. Ed.*, 2019, **58**, 12138–12142.

27 P. Zhu, J. Wang, F. Xia, W. Zhang, H. Liu and X. Zhang, Alcohol-Assisted Synthesis of Sheet-Like ZSM-5 Zeolites with Controllable Aspect Ratios, *Eur. J. Inorg. Chem.*, 2023, e202200664.

28 X. Chen, W. Yan, W. Shen, J. Yu, X. Cao and R. Xu, Morphology control of self-stacked silicalite-1 crystals using microwave-assisted solvothermal synthesis, *Microporous Mesoporous Mater.*, 2007, **104**, 296–304.

29 J. Yu, K. Du, D. Pan, H. Li, L. Ding, W. Chen, Y. Zhang and Y. Tang, Distinguishing and unraveling classical and non-classical pathways in MFI zeolite crystallization: insights into their contributions and impact on the final product, *Inorg. Chem. Front.*, 2025, **12**, 4048–4058.

30 K. Góra-Marek, K. Tarach and M. Choi, 2,6-Di-tert-butylpyridine Sorption Approach to Quantify the External Acidity in Hierarchical Zeolites, *J. Phys. Chem. C*, 2014, **118**, 12266–12274.

31 H. Shen, M. Liu, J. Li, X. Li, S. Xie, F. Chen, L. Xu, X. Guo, C. Song and X. Zhu, Promising Strategy to Synthesize ZSM-5@Silicalite-1 with Superior Catalytic Performance for Catalytic Cracking Reactions, *Ind. Eng. Chem. Res.*, 2021, **60**, 9098–9106.

32 F. Wang, X. Wang, Z. Li, J. Ma, W. Dai, J. Zheng and R. Li, Zeolite-modified alumina-bead catalyst for hierarchical cracking of bulky molecules, *Colloids Surf., A*, 2024, **703**, 135316.

33 L. Ren, Q. Wu, C. Yang, L. Zhu, C. Li, P. Zhang, H. Zhang, X. Meng and F.-S. Xiao, Solvent-Free Synthesis of Zeolites from Solid Raw Materials, *J. Am. Chem. Soc.*, 2012, **134**, 15173–15176.

34 H. Li, J. Yu, K. Du, W. Li, L. Ding, W. Chen, S. Xie, Y. Zhang and Y. Tang, Synthesis of ZSM-5 Zeolite Nanosheets with Tunable Silanol Nest Contents across an Ultra-wide pH Range and Their Catalytic Validation, *Angew. Chem., Int. Ed.*, 2024, **63**, e202405092.

35 M. D. Foster, I. Rivin, M. M. J. Treacy and O. Delgado Friedrichs, A geometric solution to the largest-free-sphere problem in zeolite frameworks, *Microporous Mesoporous Mater.*, 2006, **90**, 32–38.

36 Z. Sheng, H. Li, K. Du, L. Gao, J. Ju, Y. Zhang and Y. Tang, Observing a Zeolite Nucleus (Subcrystal) with a Uniform Framework Structure and Its Oriented Attachment without Single-Molecule Addition, *Angew. Chem., Int. Ed.*, 2021, **60**, 13444–13451.

37 Y.-Q. Deng, W.-F. Zhou, H.-M. Lv, Y.-Y. Zhang, C.-T. Au and S.-F. Yin, Synthesis of HZSM-5@silicalite-1 core–shell composite and its catalytic application in the generation of p-xylene by methylation of toluene with methyl bromide, *RSC Adv.*, 2014, **4**, 37296–37301.

38 X. Pan, X. Huang, R. Wang, H. Zhang, H. Wei, J. Chen, S. Liu, L. Sun, D. Xu and Y. Liu, Effects of Silicalite-1 Coating on the p-Xylene Selectivity and Catalytic Stability of HZSM-5 in Toluene Methylation with Methanol, *Catalysts*, 2022, **12**, 1538.

39 T. T. Le, K. Shilpa, C. Lee, S. Han, C. Weiland, S. R. Bare, P. J. Dauenhauer and J. D. Rimer, Core-shell and egg-shell zeolite catalysts for enhanced hydrocarbon processing, *J. Catal.*, 2022, **405**, 664–675.

40 F. Wei, J.-P. Cao, J.-P. Zhao and X.-Y. Zhao, Acidity-Tuned ZSM-5@Silicalite-1 Core–Shell Catalysts for Upgrading Lignite Pyrolysis Volatiles to Light Aromatics, *Fuel*, 2025, **399**, 135601.

41 S. Li, J. Li, M. Dong, S. Fan, T. Zhao, J. Wang and W. Fan, Strategies to control zeolite particle morphology, *Chem. Soc. Rev.*, 2019, **48**, 885–907.

42 Z. Zhang, Y. Sun, H. Zhang and L. Wei, Synthesis, Types, and Applications of Zeolite Capsule Catalysts, *Cryst. Res. Technol.*, 2023, **58**, 2200287.

43 D. Hao, X. Li, G. He, R. Bai, Y. Bai, T. Zhang, L. Bai, J. Li, Q. Zhang, D. Mei, Z. Feng and J. Yu, Ethanol-assisted

synthesis of titanium-rich TS-1 zeolite: a new hexa-coordinated Ti site for efficient propylene epoxidation, *Chem. Sci.*, 2025, **16**, 4661–4667.

44 C.-H. Cheng and D. F. Shantz, Silicalite-1 Growth from Clear Solution: Effect of Alcohol Identity and Content on Growth Kinetics, *J. Phys. Chem. B*, 2005, **109**, 19116–19125.

45 Y. Huang, J. Yao, X. Zhang, C. Kong, H. Chen, D. Liu, M. Tsapatsis, M. R. Hill, A. J. Hill and H. Wang, Role of ethanol in sodalite crystallization in an ethanol–Na_2O–Al_2O_3–SiO_2–H_2O system, *CrystEngComm*, 2011, **13**, 4714–4722.

46 D. P. Petry, M. Haouas, S. C. C. Wong, A. Aerts, C. E. A. Kirschhock, J. A. Martens, S. J. Gaskell, M. W. Anderson and F. Taulelle, Connectivity Analysis of the Clear Sol Precursor of Silicalite: Are Nanoparticles Aggregated Oligomers or Silica Particles?, *J. Phys. Chem. C*, 2009, **113**, 20827–20836.

47 M. Castro, M. Haouas, F. Taulelle, I. Lim, E. Breynaert, G. Brabants, C. E. A. Kirschhock and W. Schmidt, Multi-diagnostic analysis of silicate speciation in clear solutions/sols for zeolite synthesis, *Microporous Mesoporous Mater.*, 2014, **189**, 158–162.

48 S. Bosnar, M. D. Sikirić, V. Smrečki, J. Bronić, S. Šegota, V. Strasser, T. Antonić Jelić, A. Palčić and B. Subotić, Controlled aggregation of core(amorphous silica)@shell(TPA^+-polysilicate) nanoparticles at room temperature by selective removal of TPA^+ ions from the nanoparticle shell, *Inorg. Chem. Front.*, 2019, **6**, 1639–1653.

49 T. M. Davis, T. O. Drews, H. Ramanan, C. He, J. Dong, H. Schnablegger, M. A. Katsoulakis, E. Kokkoli, A. V. McCormick, R. L. Penn and M. Tsapatsis, Mechanistic principles of nanoparticle evolution to zeolite crystals, *Nat. Mater.*, 2006, **5**, 400–408.

50 A. Aerts, L. R. A. Follens, M. Haouas, T. P. Caremans, M.-A. Delsuc, B. Loppinet, J. Vermant, B. Goderis, F. Taulelle, J. A. Martens and C. E. A. Kirschhock, Combined NMR, SAXS, and DLS Study of Concentrated Clear Solutions Used in Silicalite-1 Zeolite Synthesis, *Chem. Mater.*, 2007, **19**, 3448–3454.

51 D. V. Vu, M. Miyamoto, N. Nishiyama, S. Ichikawa, Y. Egashira and K. Ueyama, Catalytic activities and structures of silicalite-1/H-ZSM-5 zeolite composites, *Microporous Mesoporous Mater.*, 2008, **115**, 106–112.

52 D. Van Vu, M. Miyamoto, N. Nishiyama, Y. Egashira and K. Ueyama, Morphology Control of Silicalite/HZSM-5 Composite Catalysts for the Formation of Para-Xylene, *Catal. Lett.*, 2009, **127**, 233–238.

53 C. Chu-Jon, E. Martinez, A. A. Bertolazzo, A. Koneru, S. K. R. S. Sankaranarayanan, J. D. Rimer and V. Molinero, From Non-classical to Classical: Crystallization Seeds Reshape Nucleation Mechanisms, *J. Am. Chem. Soc.*, 2025, **147**, 20456–20465.